Supplementary Information

Sensitive, high-throughput, metabolic analysis by molecular sensors on the membrane surface of mother yeast cells (MOMS)

Wenxin JIANG[1], Xingjie HUANG[1], Huanmin DU[1], Luke P. LEE[2,3,4]*,

and Chia-Hung CHEN[1]*

[1]Department of Biomedical Engineering, City University of Hong Kong, 83 Tat Chee Avenue, Hong Kong SAR, China

[2]Harvard Medical School, Harvard University; Department of Medicine, Brigham and Women's Hospital, Boston, MA 02115, USA

[3]Department of Bioengineering, Department of Electrical Engineering and Computer Science, University of California, Berkeley, Berkeley, CA 94720, USA

[4]Department of Biophysics, Institute of Quantum Biophysics, Sungkyunkwan University, Suwon, Korea

* Luke P. LEE

Email: lplee@bwh.harvard.edu

* Chia-Hung CHEN

Email: chiachen@cityu.edu.hk

This PDF file includes:

Supplementary Figs. 1-18

Supplementary Tables 1-6

Supplementary References

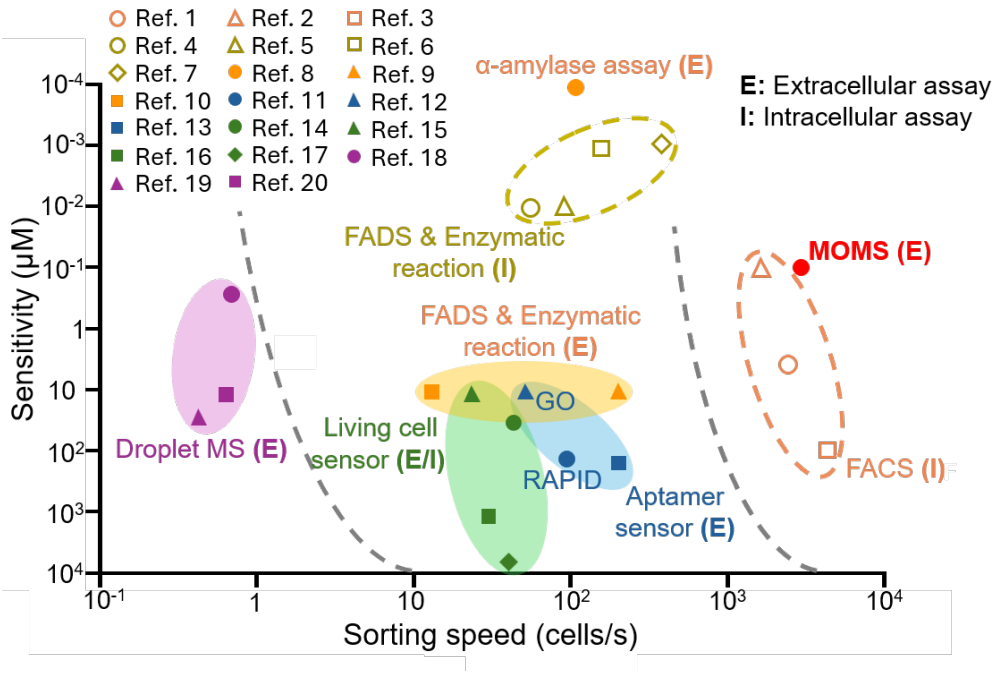

Supplementary Fig. 1. Comparative analysis of droplet screening technologies: In contrast to many other droplet screening methods aimed at detecting intracellular molecules or extracellular secretions of microbes, MOMS offer a >10-fold improvement in extracellular secretion assay sensitivity and a >30-fold enhancement in sorting speed of secreted strains[1-20].

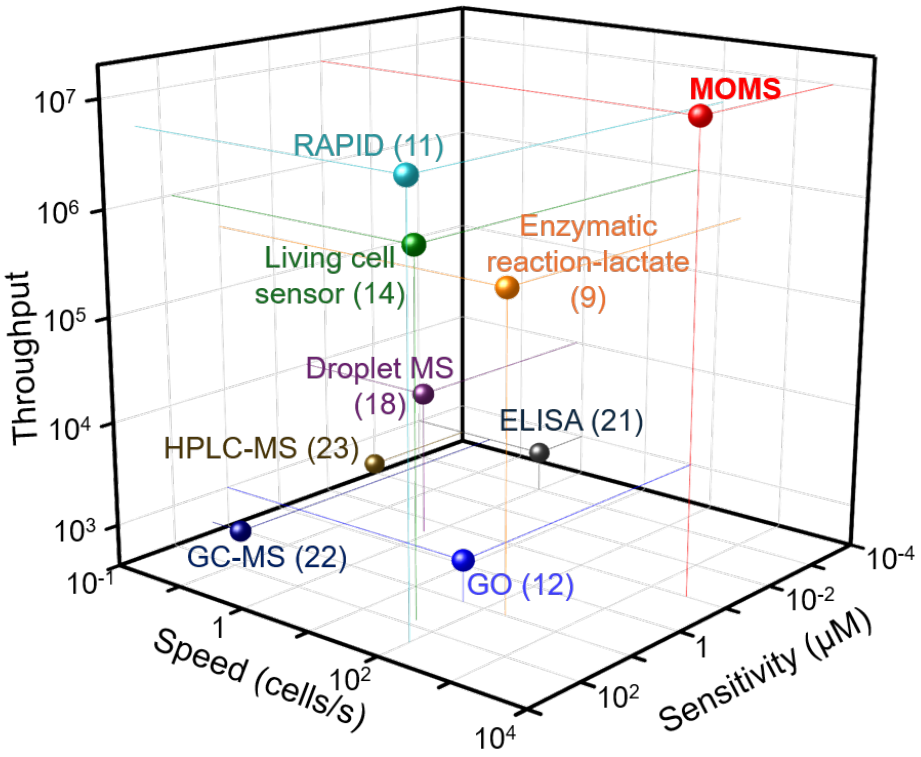

Supplementary Fig. 2. Comparative analysis of extracellular metabolite secretion assay: Compared to previous technologies for measuring single-microbe extracellular metabolite secretion, MOMS is the optimized molecular sensing system, offering significant advantages in high sensitivity, high screening throughput, and ultra-fast sorting speed[9, 11, 12, 14, 18, 21-23].

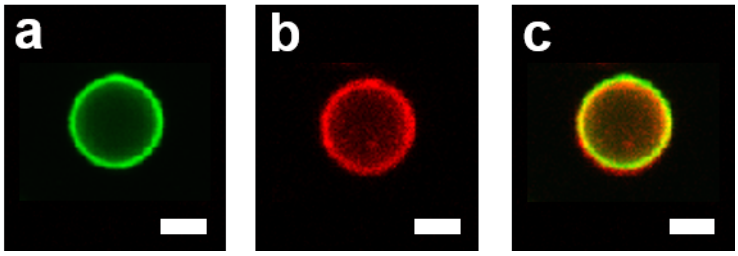

Supplementary Fig. 3. MOMS coating on yeast cell surface: Confocal laser scanning microscopy (CLSM) images of a single yeast cell coated with fluorescently tagged single-stranded DNA (biotin-VANapt-Cy5), and subsequently incubated with Alexa Fluor 488 labeled Concanavalin A (ConA). The images demonstrated aptamer localization exclusively on the cell surface: (a) The yeast cell wall was visualized after the binding of Alexa Fluor 488 labeled ConA (excitation: 495 nm, emission: 515 nm). (b) The successful coating of MOMS on single yeast cell was observed by Cy5 fluorescence (excitation: 646 nm, emission: 664 nm). (c) A merged image of Alexa Fluor 488 and Cy5 fluorescence indicated that MOMS coating only happened on the yeast cell surface (scale bar: 2.0 μm).

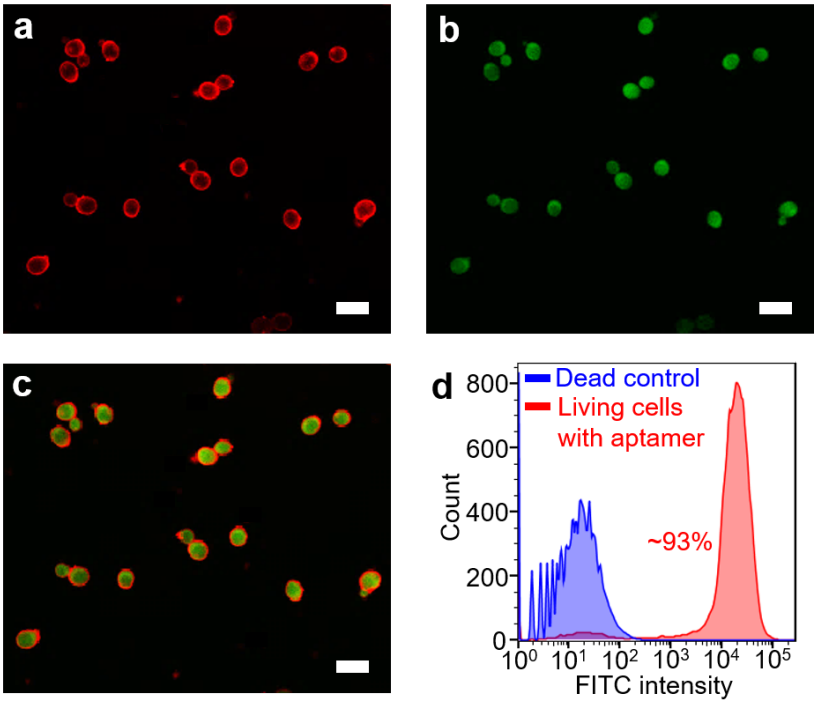

Supplementary Fig. 4. Cell viability test after MOMS coating: CLSM images and flow cytometry analysis of yeast cells coated with biotin-VANapt-Cy5 and subsequently treated with fluorescein diacetate (FDA, 25 µg/mL), confirming high cell viability. (a) MOMS coating was visualized under CLSM using Cy5 fluorescence labeling (excitation: 656 nm, emission: 664 nm), confirming successful coating on yeast cells. (b) FDA live-dead staining, which detects esterase activity in living cells, was used to assess cell viability under CLSM (excitation: 490 nm, emission: 525 nm). (c) A merged image of Cy5 and fluorescein fluorescence was obtained, further validating yeast cell integrity (scale bar: 8.0 µm). (d) Flow cytometry analysis demonstrated 93% yeast cell viability after MOMS coating, confirming its biocompatibility.

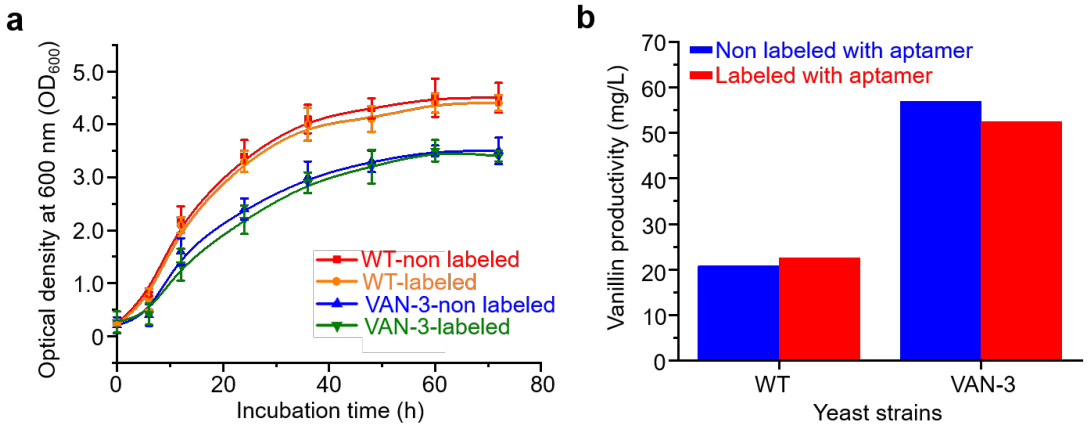

Supplementary Fig. 5. Biocompatibility of MOMS coating: (a) A cell growth curve test was conducted to confirm that MOMS coating did not affect yeast cell growth across different strains. WT strains were cultured in 5 mL of SD medium with an initial OD_{600} of ~0.2 and incubated at 30°C with shaking at 250 rpm. For VAN-3 strains, the medium was supplemented with 1.0 g/L ferulic acid. (b) The vanillin productivity test of WT and VAN-3 yeast strains, with and without MOMS coating, was performed using an established absorbance-based method. The results demonstrated no significant difference in vanillin production, confirming the biocompatibility of the MOMS system.

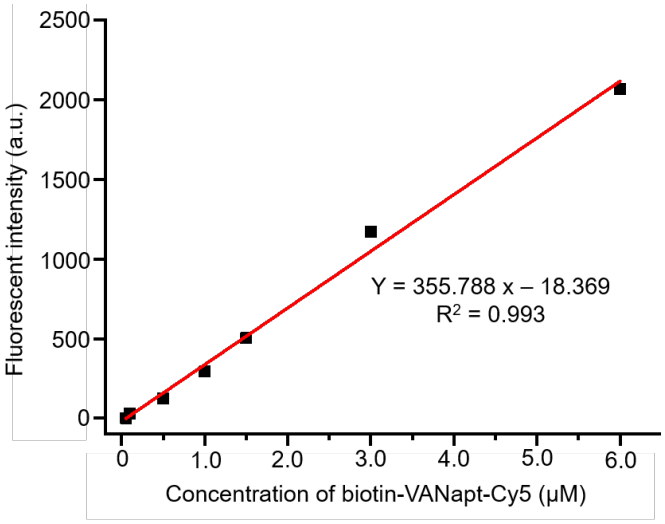

Supplementary Fig. 6. Fluorescence calibration for quantifying aptamer concentration: A calibration curve was generated by plotting fluorescence intensity in solution against the concentration of biotin-VANapt-Cy5. It was used to evaluate the average number of MOMS coated on the surface of single yeast cells.

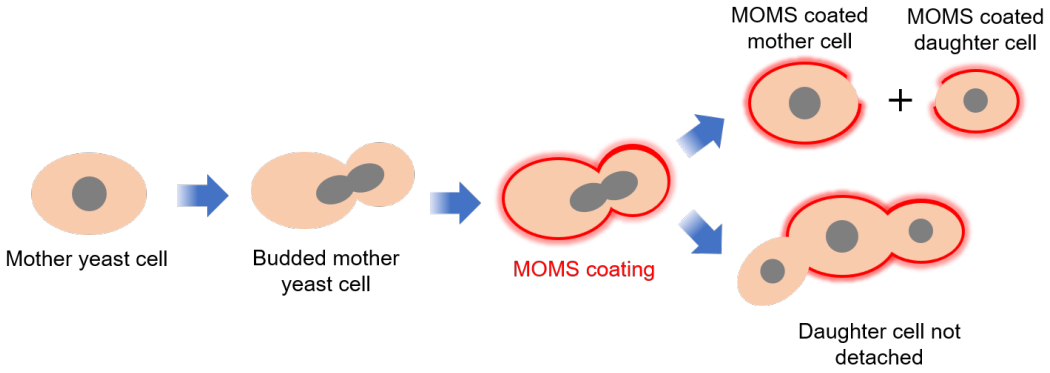

Supplementary Fig. 7. MOMS coating during yeast budding: A schematic illustrates that some yeast cells may initiate the budding process prior to MOMS coating, leading to a slight decrease and fluctuation in fluorescence signal on yeast cell surfaces. Nevertheless, the high MOMS sensor density remains on the majority of mother yeast cells, ensuring sensitive secretion measurements.

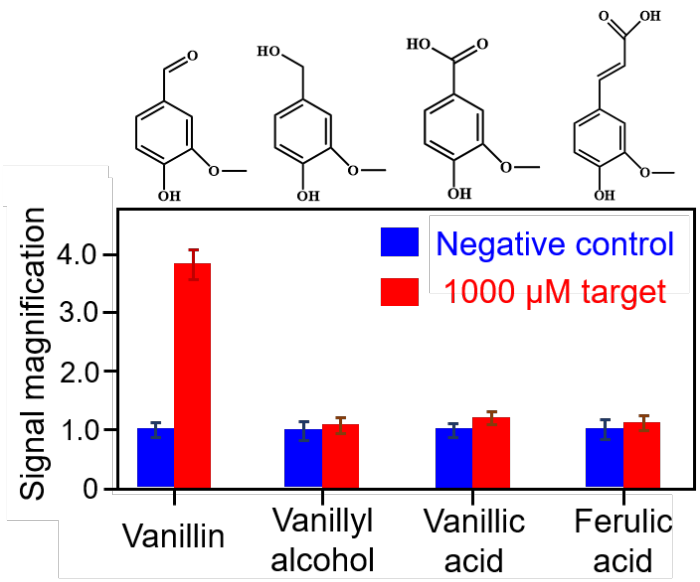

Supplementary Fig. 8. Specificity tests of MOMS: A specificity assay was conducted on vanillin-targeted MOMS-coated yeast cells exposed to 1 mM vanillin, vanillyl alcohol, vanillic acid, and ferulic acid, demonstrating a high specificity ratio (3.45-fold) for vanillin.

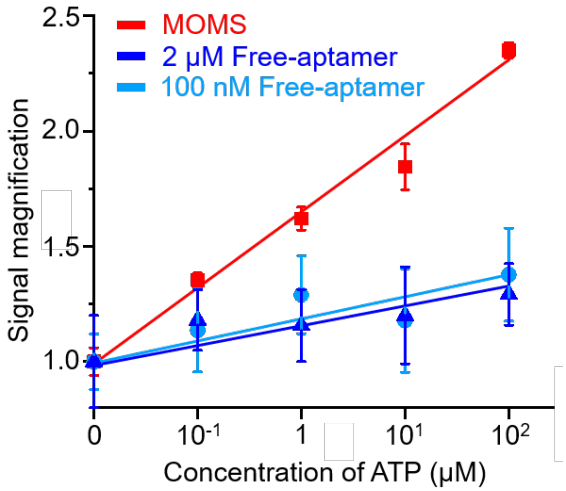

Supplementary Fig. 9. Sensitivity comparison between MOMS and free-floating aptamer sensors: To validate MOMS' sensitivity advantage, we compared ATP-targeted MOMS with free-floating ATP aptamer sensors. Free-floating aptamers (100 nM or 2 μM) were co-incubated with uncoated yeast cells (2.0 × 10^7 cells/mL), a blocking agent (0.1 mg/mL herring sperm DNA), and varying ATP concentrations, with fluorescence signals measured using a microplate reader. Unlike MOMS, which showed clear fluorescence increases, free-floating aptamers exhibited fluctuating signal changes across ATP concentrations (100 nM to 10 μM), due to non-specific interactions causing high background noise. In contrast, MOMS immobilization reduces non-specific binding, enhances stability, and improves detection sensitivity.

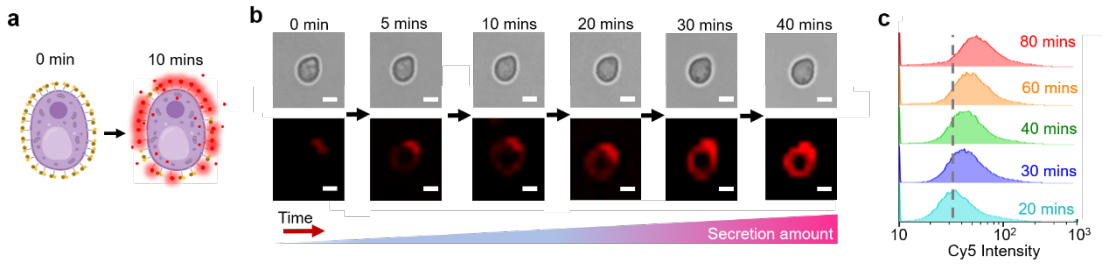

Supplementary Fig. 10. Sensitive secretion measurement over time: (a) Schematic illustration of MOMS-coated yeast cells capturing their own secretions directly on the cell surface, enabling rapid detection of secreted molecules. (b) Time-lapse visualization of ATP secretion from single yeast cells captured by MOMS, monitored using LCSM. Images were taken every 5 minutes over a 40-minute period (scale bar: 2.0 μm). (c) Flow cytometry analysis showing a progressive increase in yeast ATP secretion over time.

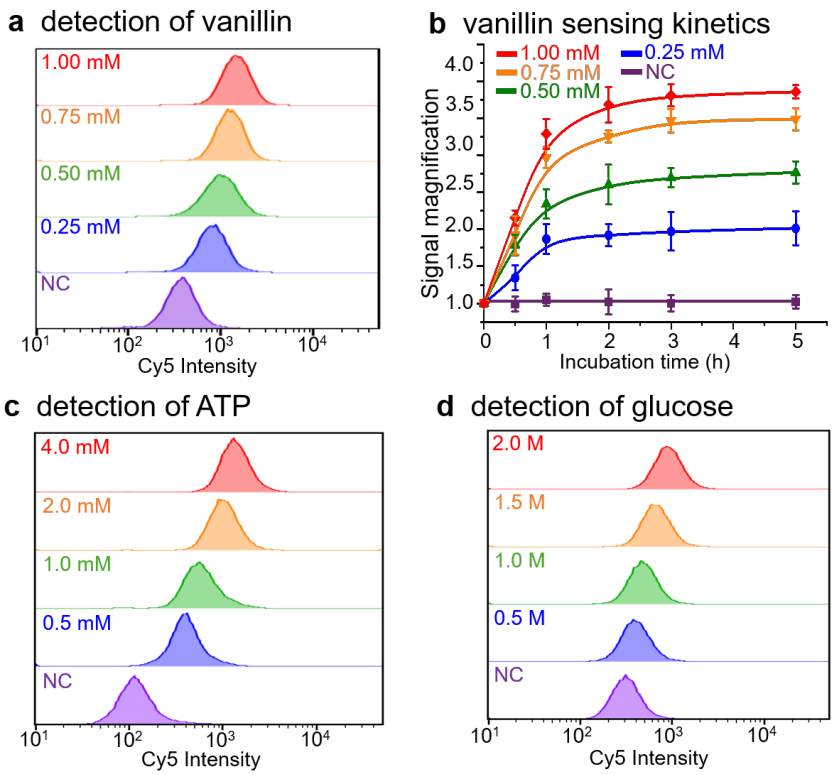

Supplementary Fig. 11. Molecular detection at different concentrations: (a) Vanillin assay – MOMS-coated yeast cells were used to detect vanillin concentrations ranging from 0 to 1.00 mM. The fluorescence signal increased from 842 a.u. to 1509 a.u. as the concentration rose from 0.25 mM to 1.00 mM, confirming a concentration-dependent response. (b) Vanillin sensing kinetics – Fluorescence intensity was monitored over time (0–5 hours) to evaluate vanillin detection kinetics. Upon adding vanillin at different concentrations (0.25–1.00 mM), fluorescence signals increased within the first hour and saturated after 2 hours. In contrast, the negative control (without vanillin) showed no fluorescence increase over time. (c) ATP assay – MOMS-coated yeast cells were used to detect ATP concentrations ranging from 0 to 4.0 mM. The fluorescence signal increased from 450 a.u. to 1472 a.u. as the ATP concentration rose from 0.5 mM to 4.0 mM, demonstrating efficient ATP sensing. (d) Glucose assay – MOMS-coated yeast cells detected glucose concentrations between 0 and 2.0 M, with fluorescence signals increasing from 433 a.u. to 966 a.u. as the glucose concentration increased from 0.5 M to 2.0 M, indicating glucose sensing.

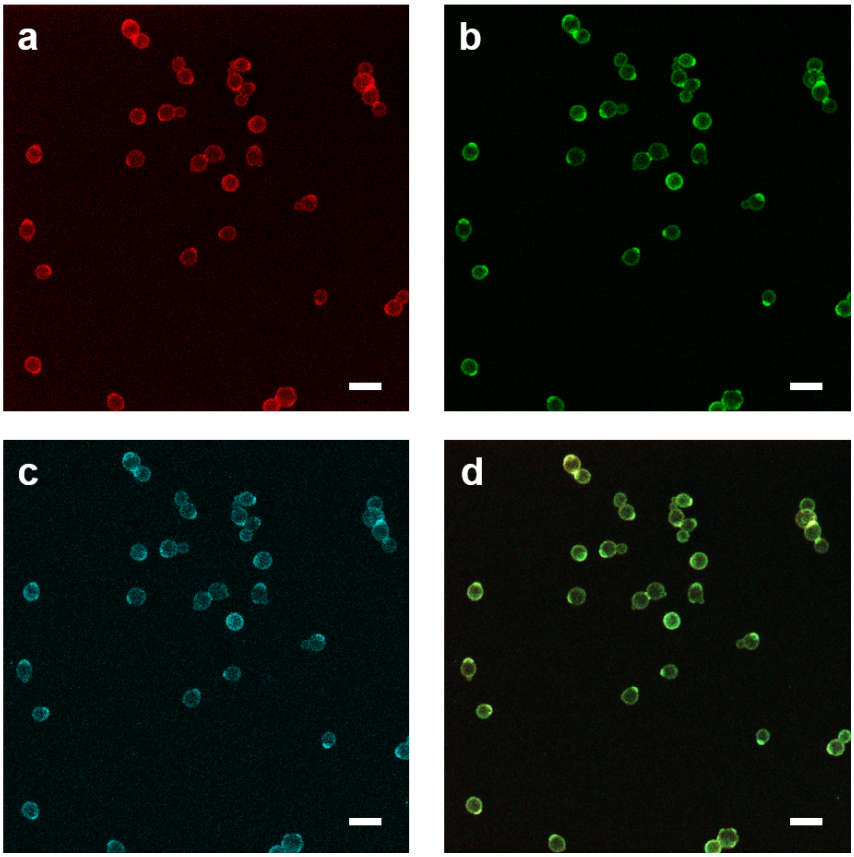

Supplementary Fig. 12. Combined MOMS coating on yeast cells: A single yeast cell was simultaneously coated with three different aptamers for multiplexed assays, visualized using LCSM. (a) MOMS containing biotin-ATPapt-Cy5 were coated on yeast cells (excitation: 646 nm, mission: 664 nm). (b) MOMS containing biotin-VANapt-FITC were coated on yeast cells (excitation: 490 nm, emission: 525 nm). (c) MOMS containing biotin-GLUapt-Cy3 were coated on yeast cells (excitation: 555 nm, emission: 570 nm). (d) Merged fluorescence channels confirmed the simultaneous coating of different MOMS on the same yeast cells (Scale bar: 10 μm).

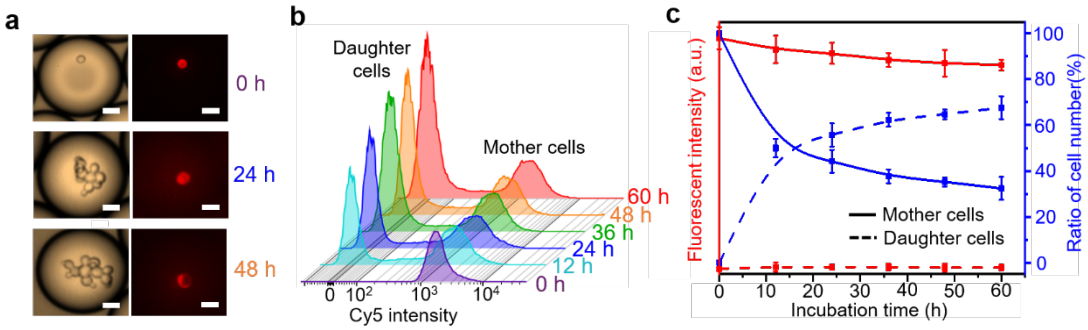

Supplementary Fig. 13. Selective MOMS coating on mother yeast cells in droplets: (a) The budding of MOMS-coated yeast cells in droplets was observed using bright-field and fluorescence microscopy, demonstrating that MOMS coatings remained on mother cells while daughter cells remained uncoated (scale bar: 6 μm). (b) Flow cytometry confirmed the high stability of MOMS coatings, which persisted on mother cells within droplets for up to 60 hours. This stability ensured a consistent sensor density for sensitive secretion detection. A high proportion of mother cells retained dense MOMS coatings, as evidenced by strong Cy5 fluorescence signals, while most daughter cells remained uncoated. (c) Flow cytometry analysis revealed that although the proportion of mother cells in the population decreased over time, the MOMS sensor density on mother yeast cells showed only a slight reduction, ensuring reliable capture of secreted molecules for assay measurements.

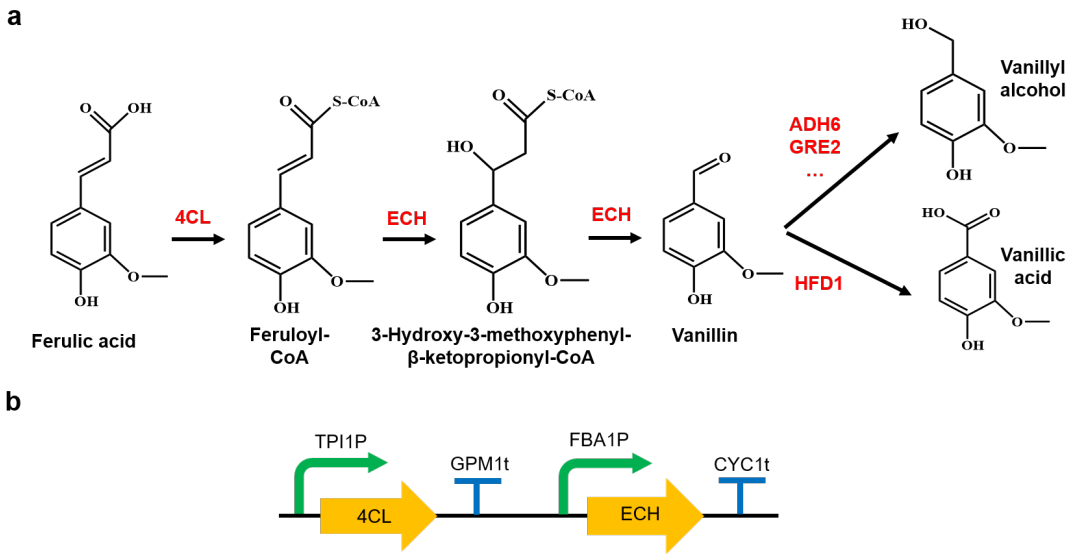

Supplementary Fig. 14. Metabolic pathway for engineering yeast to produce vanillin: (a) Schematic representation of the vanillin biosynthesis pathway from ferulic acid. In *S. cerevisiae* BY4742, native enzymes can convert vanillin into vanillyl alcohol or vanillic acid, reducing its accumulation[24]. To enhance extracellular vanillin secretion, we constructed a series of engineered yeast strains (VAN-1, VAN-2, and VAN-3) designed to suppress vanillin reduction, thereby increasing productivity. (b) Gene circuit in plasmid pCYP-VAN, which harbors the *4cl* and *ech* genes essential for vanillin synthesis.

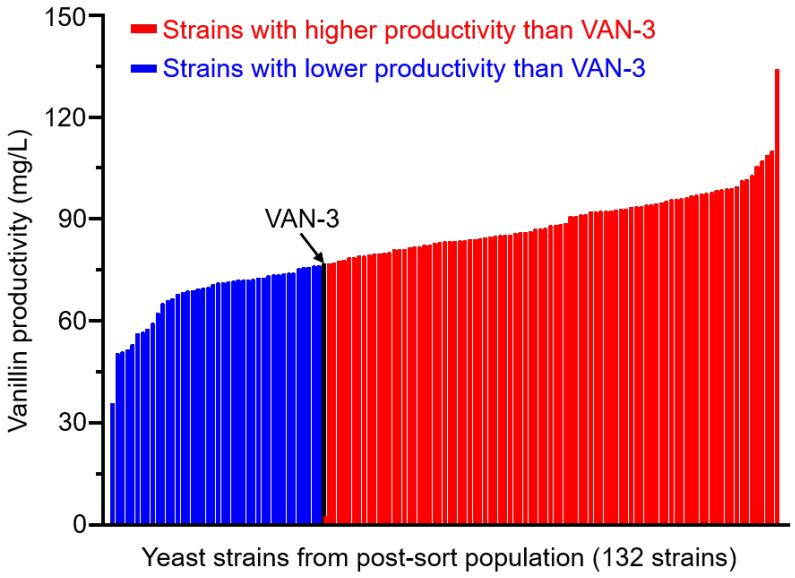

Supplementary Fig. 15. Validation of vanillin production via absorbance measurements: Absorbance measurements were performed using a microplate reader to assess vanillin production in sorted yeast cells cultured in micro-wells. Vanillin productivity was determined by measuring the optical density at 438 nm (OD_{438}). From the post-sorting population (301 strains in total), 132 yeast strains were randomly selected for evaluation. Among them, 90 strains exhibited higher productivity than the control strain (VAN-3), demonstrating a sorting accuracy of approximately 68% for the directed evolution of ECH.

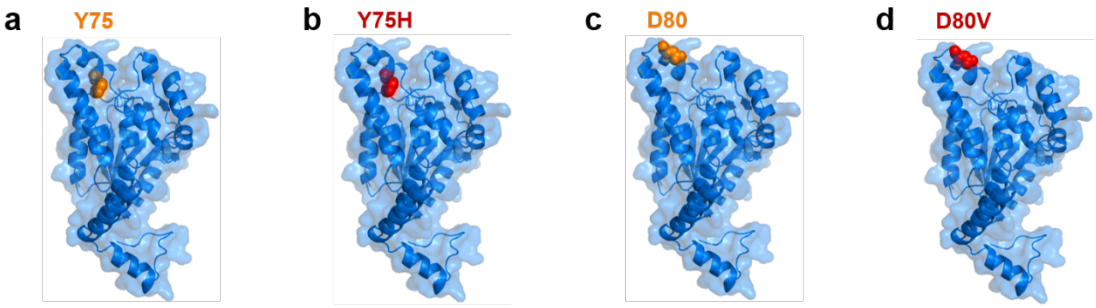

Supplementary Fig. 16. Additional mutation sites in ECH variants from sorted strains: (a) Schematic of the original ECH structure, highlighting the amino acid Y75. (b) Schematic of the sorted mutational ECH from S-8 strain, with the Y75H substitution highlighted in red. (c) Schematic of the original ECH structure, highlighting the amino acid D80. (d) Schematic of the sorted mutational ECH variant from S-1 strain, with the D80V substitution highlighted in red.

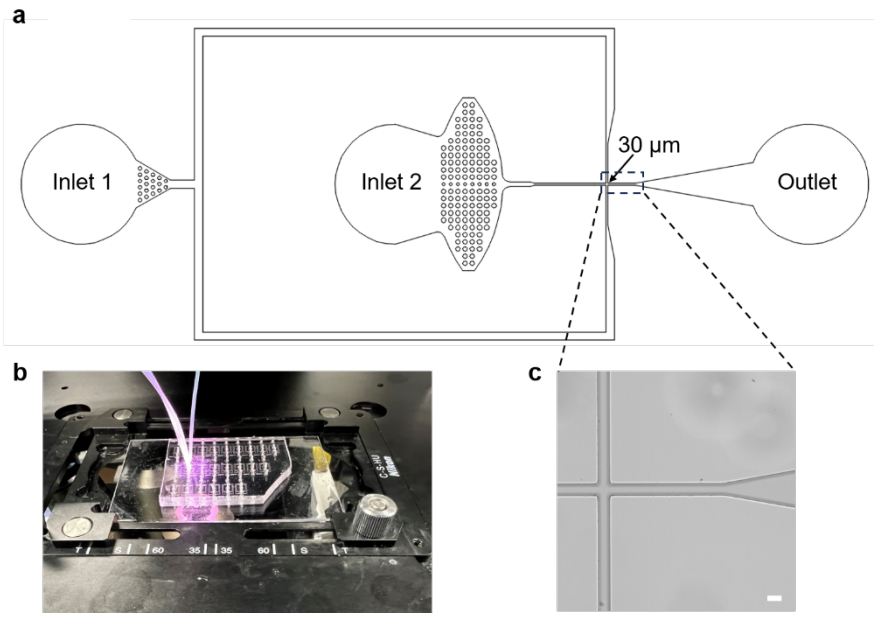

Supplementary Fig. 17. Microfluidic device: (a) Schematic of the microfluidic droplet generator (30-µm width and 40-µm height at the nozzle), used to produce 40-µm droplets for single yeast cell encapsulation and incubation. The oil phase was introduced through inlet 1 at a flow rate of 5.0×10^3 µL/h, while the yeast cell suspension was loaded into inlet 2 at a flow rate of 600 µL/h. (b) Photograph of the polydimethylsiloxane (PDMS) device designed for water-in-oil droplet generation. (c) Bright-field image of the nozzle in microfluidic channel for droplet generation (scale bar: 30 µm).

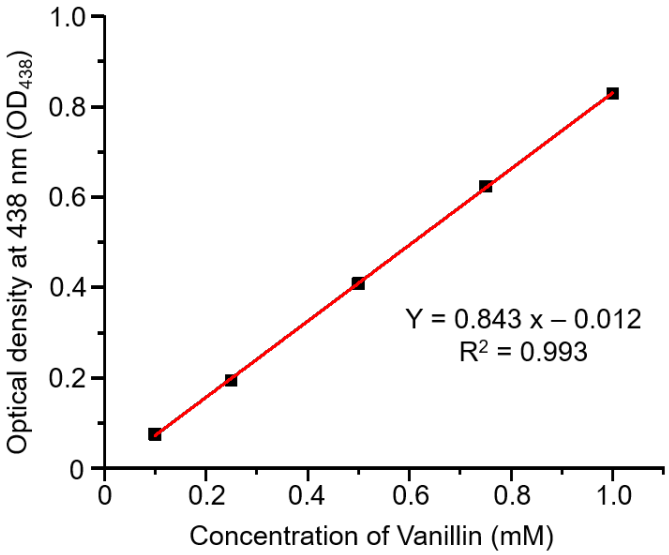

Supplementary Fig. 18. Vanillin concentration calibration by absorbance: The OD_{438} was measured for solutions with varying vanillin concentrations to establish a calibration curve for quantifying vanillin concentration.

Supplementary Table 1. Comparative analysis of main droplet screening technologies for detection of single microbe intracellular products or extracellular secretions.

Platform	Target	Sensitivity	Sorting speed (cells/s)	Ref.
FACS for intracellular assay	Theophylline	10 μM	~10^3–10^4	1
	Oleic acid	100 nM	~10^3–10^4	2
	Alkanes	240 μM	~10^3–10^4	3
Enzymatic reaction in droplet for intracellular assay	Arylsulfatase	10 nM	~60	4
	Archaeoglobus fulgidus esterase	10 nM	~100	5
	Phosphotriesterase	2.5 nM	~200	6
	Horseradish peroxidase	1.0 nM	~440	7
Enzymatic reaction in droplet for extracellular assay	α-Amylase	0.1 nM	~120	8
	Lactate	10 μM	~200	9
	Ethanol	10 μM	~15	10
Aptamer sensor in droplet for extracellular assay	Tyrosine	260 μM	~100	11
	Naringenin	10 μM	~50	12
	Tryptophan	313 μM	~200	13
Living cell sensor in droplet for extracellular and intracellular assay	Naringenin	70 μM	~45	14
	2-Ketoisovalerate	14 μM	~25	15
	Glucosamine	1 mM	~30	16
	D-allulose	10 mM	~40	17
Droplet mass spectrometry for extracellular assay	Ethyl-3-hydroxybutyrate	250 nM	~0.8	18
	Lysine	80 μM	~0.5	19
	Ketone 1-(imidazo[2,1 b]thiazol-6-yl) propan-2-one	30 μM	~0.7	20
This work: MOMS	ATP Vanillin Glucose	100 nM 100 nM 1 μM	~3.0×10^3	–

Supplementary Table 2. Comparative analysis of main technologies for single microbe secretion analysis.

Platform	Sensitivity	Screening throughput (cells/assay)	Sorting speed (cells/s)
Enzyme linked immunosorbent assay (ELISA)[21]	1 nM	~10^3–10^4	~1
Gas chromatography–mass spectrometry (GC-MS)[22]	20 μM	~10^2–10^3	~0.03
High-performance liquid chromatography–mass spectrometry (HPLC-MS)[23]	1 nM	~10^2–10^3	~0.05
Enzymatic reaction in droplet for lactate detection[9]	10 μM	~4.0×10^5	~200
RNA-Aptamer-in-Droplet (RAPID)[11]	260 μM	~5.0×10^6	~100
graphene oxide (GO) aptasensors in droplet[12]	10 μM	~10^3–10^4	~50
Living cell sensors in droplet[14]	70 μM	~10^6	~10
Droplet mass spectrometry (MS)[18]	250 nM	~10^4	0.8
This work: MOMS	100 nM	~1.0×10^7	~3000

Supplementary Table 3. The aptamer sequences and details.

Name	Description	Sequences (5'-3')
Biotin-VANapt-Cy5[25]	Vanillin aptamer labeled by Cy5	/Biotin/SpacerC9/CAGGAGAAACATGGAGTCTCGATGAT/Cy5/
BHQ3-VANQ	Quenching cDNA to Biotin-VANapt-Cy5	/BHQ3/TCATCGAGAC
Biotin-VANapt-FITC	Vanillin aptamer labeled by FITC	/Biotin/SpacerC9/CAGGAGAAACATGGAGTCTCGATGAT/FITC/
BHQ1-VANQ	Quenching cDNA to Biotin-VANapt-FITC	/BHQ1/TCATCGAGAC
Biotin-ATPapt-Cy5[26]	ATP aptamer labeled by Cy5	/Cy5/TACCTGGGGGAGTATTGCGGAGGAAGGT/SpacerC9/Biotin/
BHQ3-ATPQ	Quenching cDNA to Biotin-ATPapt-Cy5	CTCCCCCAGGTA/BHQ3/
Biotin-GLUapt-Cy5[27]	D-glucose aptamer labeled by Cy5	/Cy5/CTCTCGGGACGACCGTGTGTGTTGCTCTGTAACAGTGTCCATTGTCGTCCC/SpacerC9/Biotin/
BHQ3-GLUQ	Quenching cDNA to Biotin-GLUapt-Cy5	GTCGTCCCGAGAG/BHQ3/
Biotin-GLUapt-Cy3	D-glucose aptamer labeled by Cy3	/Cy3/CTCTCGGGACGACCGTGTGTGTTGCTCTGTAACAGTGTCCATTGTCGTCCC/SpacerC9/Biotin/
BHQ2-GLUQ	Quenching cDNA to Biotin-GLUapt-Cy3	GTCGTCCCGAGAG/BHQ2/
Biotin-ZINapt-Cy5[28]	Zinc ion aptamer labeled by Cy5	/Cy5/CCATCAGTTAGTCATTACGCTTACGGCGGCTCTATCCTAACTGATATATTGTGAAGTCGTGTCCC/SpacerC9/Biotin/
BHQ3-ZINQ	Quenching cDNA to Biotin-ZINapt-Cy5	ATGACTAACTGATGG/BHQ3/
Biotin-NC-Cy5[29]	Negative control DNA labeled by Cy5	/Biotin/SpacerC9/CTCATTCAATACCCTACGTCTACCCTAC/Cy5/
BHQ3-NCQ	Quenching cDNA to Biotin-NC-Cy5	/BHQ3/GTAGGGTAGACG
Biotin-NC-FITC	Negative control DNA labeled by FITC	/Biotin/SpacerC9/CTCATTCAATACCCTACGTCTACCCTAC/FITC/
BHQ1-NCQ	Quenching cDNA to Biotin-NC-FITC	/BHQ1/GTAGGGTAGACG

Supplementary Table 4. The strains used in this study.

Strains	**Description**	**Source**
E. coli DH5α	Host for construction of plasmids	Sangon
E. coli Trans1-T1	Host for construction of mutation library	TransGen
S. cerevisiae BY4742	Host for vanillin production	Beijing Zoman
D-1	BY4742 derivate, Δ*gre2*	This study
D-2	BY4742 derivate, Δ*adh6*	This study
D-3	BY4742 derivate, Δ*gre2*, Δ*adh6*	This study
VAN-1	D-1 harboring pVAN	This study
VAN-2	D-2 harboring pVAN	This study
VAN-3	D-3 harboring pVAN	This study
WT	D-3 harboring pYCP	This study
S-1	D-3 harboring pVAN^{D80V}	This study
S-8	D-3 harboring pVAN^{Y75H}	This study
S-10	D-3 harboring pVAN$^{I90N/Y169C/N212Q/P213L}$	This study

Supplementary Table 5. The plasmids used in this study.

Plasmids	**Description**	**Source**
pYCP	*E. coli–S. cerevisiae* shuttle vector with Amp^R and LEU2 markers	VectorBuilder
pML104	*E. coli–S. cerevisiae* shuttle vector with Amp^R and URA3 markers, expressing Cas9 and containing single guide RNA (sgRNA) expression cassette	Addgene
pML104-*adh6*	pML104 derivate, containing the sgRNA for *adh6* gene deletion	This study
pML104-*gre2*	pML104 derivate, containing the sgRNA for *gre2* gene deletion	This study
pVAN	pYCP derivate, containing the expression cassettes for 4cl and ech genes: P_{TPI1}-*4cl*-T_{GPM1}-P_{FBA1}-*ech*-T_{CYC1}	This study
$pVAN^{D80V}$	pVAN derivate, with mutation sites D80V in *ech* gene	This study
$pVAN^{Y75H}$	pVAN derivate, with mutation sites Y75H in *ech* gene	This study
$pVAN^{I90N/Y169C/N212Q/P213L}$	pVAN derivate, with mutation sites I90N/Y169C/N212Q/P213L in *ech* gene	This study

Supplementary Table 6. The primers used in this study[24].

Name	Sequence (5'-3')
Primers for deletion of *gre2* and *adh6* genes in *S. cerevisiae* BY4742	
ADH6-sgRNA-F	GATCGACATTAAGATCGAAGCATGTGGGTTTTAGAGCTAG
ADH6-sgRNA-R	CTAGCTCTAAAACCCACATGCTTCGATCTTAATGTC
ADH6-donorU-F	GGACCTTGACGTGGAATTCC
ADH6-donorU-R	GGCTTTTCTTGTTGTTGTGTTG
ADH6-donorD-F	CAGACTAGGTTGTCAAGCTCTTG
ADH6-donorD-R	CATGGAACATCCTCATCCGC
GRE2-sgRNA-F	GATCAAAGGCCGAGAATTTAACGGGTTTTAGAGCTAG
GRE2-sgRNA-R	CTAGCTCTAAAACCCGTTAAATTCTCGGCCTTT
GRE2-donorU-F	TGTACGCTATAGTTTCCTTTCAA
GRE2-donorU-R	TTTACGGGCGTGTGATACTG
GRE2-donorD-F	TCGTCCTTCTTGAAGTCCCA
GRE2-donorD-R	CGACACTGCCTCCCAAATTT
Primers for construction of pVAN plasmid	
PTPI1-F	AACTTTGTATAGAAAAGTTGAAGGATGAGCCAAGAATAAG
PTPI1-R	TACAAACTTGTTTTAGTTTATGTATGTGTTTTTTGTAG
4CL-F	TAAACTAAAACAAGTTTGTACAAAAAAGCAG
4CL-R	TTCTTCAGACTTATTTTGGAAGGTCCCC
TGPM1-F	TCCAAAATAAGTCTGAAGAATGAATGATTTG
TGPM1-R	CAGTTGGATCTATTGCTATAACATGTCATGTC
PFBA1-F	TATAGCAATAGATCCAACTGGCACCGCTG
PFBA1-R	ATTTGCTCATTTTGAATATGTATTACTTGGTTATGGTTATATA TGACAAAAGAAAAAG
ECH-F	CATATTCAAAATGAGCAAATACGAAGGAC
ECH-R	TTTGTACAAGAAAGCTGGGTTCACCTCTTGTAAGCCTG
pYCP-F	ACCCAGCTTTCTTGTACAAAG
pYCP-R	CAACTTTTCTATACAAAGTTGGTG
4CL-colony-F	TGAGAGTGAGATGCCTGAAGTT
4CL-colony-R	ATTGCTTTATCTCCTCCTCCGT
ECH-colony-F	TTTTCCTTCTTCTTCGCCCAC
ECH-colony-R	TAGTCCTCGTTCTGTTCCCAC
Primers for construction of mutation library	
epECH-F	GTTCTTCCTTGCGTTATTCTTCTGTTCTTC
epECH-R	CACTTTGTACAAGAAAGCTGGGTTCAC
pYCP-L-F	GTGAACCCAGCTTTCTTGTACAAAGTG
pYCP-L-R	GAAGAACAGAAGAATAACGCAAGGAAGAAC

Supplementary References

1. Michenera, J. K. & Smolke, C. D. High-throughput enzyme evolution in *Saccharomyces cerevisiae* using a synthetic RNA switch. *Metab. Eng.* **14**, 306-316 (2012).
2. Zhang, F., Carothers, J. M. & Keasling, J. D. Design of a dynamic sensor-regulator system for production of chemicals and fuels derived from fatty acids. *Nat. Biotechnol.* **30**, 354-U166 (2012).
3. Chen, D. et al. Directly evolved AlkS-based biosensor platform for monitoring and high-throughput screening of alkane production. *ACS Synth. Biol.* **12**, 832-841 (2023).
4. Kintses, B. et al. Picoliter cell lysate assays in microfluidic droplet compartments for directed enzyme evolution. *Chem. Biol.* **19**, 1001-1009 (2012).
5. Ma, F. et al. Efficient molecular evolution to generate enantioselective enzymes using a dual-channel microfluidic droplet screening platform. *Nat. Commun.* **9**, 1030 (2018).
6. Colin, P.-Y. et al. Ultrahigh-throughput discovery of promiscuous enzymes by picodroplet functional metagenomics. *Nat. Commun.* **6**, 10008 (2015).
7. Agresti, J. J. et al. Ultrahigh-throughput screening in drop-based microfluidics for directed evolution. *Proc. Natl. Acad. Sci. U.S.A.* **107**, 4004-4009 (2010).
8. Sjostrom, S. L. et al. High-throughput screening for industrial enzyme production hosts by droplet microfluidics. *Lab Chip* **14**, 806-813 (2014).
9. Hammar, P. et al. Single-cell screening of photosynthetic growth and lactate production by cyanobacteria. *Biotechnol. Biofuels* **8**, 193 (2015).
10. Abalde-Cela, S. et al. High-throughput detection of ethanol producing cyanobacteria in a microdroplet platform. *J. R. Soc. Interface* **12**, 20150216 (2015).
11. Abatemarco, J. et al. RNA-aptamers-in-droplets (RAPID) high-throughput screening for secretory phenotypes. *Nat. Commun.* **8**, 332 (2017).
12. Zheng, D. et al. Graphene oxide aptasensor droplet assay for detection of metabolites secreted by single cells applied to synthetic biology. *Lab Chip* **24**, 137-147 (2024).
13. Scheele, R. A. et al. Ultrahigh throughput evolution of tryptophan synthase in droplets via an aptamer sensor. *ACS Catal.* **14**, 6259-6271 (2024).
14. Bowman, E. K. et al. Sorting for secreted molecule production using a biosensor-in-microdroplet approach. *Proc. Natl. Acad. Sci. U.S.A.* **113**, E7383-E7389 (2016).
15. Saleski, T. E. et al. Syntrophic co-culture amplification of production phenotype for high throughput screening of microbial strain libraries. *Metab. Eng.* **54**, 232-243 (2019).
16. Sun, G. et al. Directed evolution of diacetylchitobiose deacetylase via high-throughput droplet sorting with a novel, bacteria-based biosensor. *Biosens. Bioelectron.* **219**, 114818 (2023).
17. Li, C. et al. Substantial improvement of an epimerase for the synthesis of D-allulose by biosensor-based high-throughput microdroplet screening. *Angew. Chem. Int. Ed.* **62**, e202216721 (2023).

18. Wink, K. et al. Quantification of biocatalytic transformations by single microbial cells enabled by tailored integration of droplet microfluidics and mass spectrometry. *Angew. Chem. Int. Ed.* **61**, e202204098 (2022).
19. Payne, E. M., Murray, B. E., Penabad, L. I., Abbate, E. & Kennedy, R. T. Mass-activated droplet sorting for the selection of lysine-producing *Escherichia coli*. *Anal. Chem.* **95**, 15716-15724 (2023).
20. Holland-Moritz, D. A. et al. Mass activated droplet sorting (MADS) enables high-throughput screening of enzymatic reactions at nanoliter scale. *Angew. Chem. Int. Ed.* **59**, 4470-4477 (2020).
21. Rogers, D. W., McConnell, E. & Greig, D. Molecular quantification of *Saccharomyces cerevisiae* α-pheromone secretion. *FEMS Yeast Res.* **12**, 668-674 (2012).
22. Knorrscheidt, A. et al. Development of 96 Mmultiple Injection-GC-MS technique and its application in protein engineering of natural and non-natural enzymatic reactions. Available at https://doi.org/10.26434/chemrxiv.10314239.v1.
23. Yin, X., Sousa, L. S., André, B., Adams, E. & Van Schepdael, A. Quantification of amino acids secreted by yeast cells by hydrophilic interaction liquid chromatography-tandem mass spectrometry. *J. Sep. Sci.* **47**, 2400318 (2024).
24. Xin, X. et al. Engineering yeast to convert lignocellulose into vanillin. *Chem. Eng. J.* **485**, 149815 (2024).
25. Mohan, H. K. S. V. et al. A highly sensitive graphene oxide based label-free capacitive aptasensor for vanillin detection. *Mater. Des.* **186**, 108208 (2020).
26. R. Nutiu, Y. Li, Structure-switching signaling aptamers. *J. Am. Chem. Soc.* **125**, 4771-4778 (2003).
27. Nakatsuka, N. et al. Aptamer–field-effect transistors overcome Debye length limitations for small-molecule sensing. *Science*, **362**, 319-324 (2018).
28. Rajendran, M. & Ellington, A. D. Selection of fluorescent aptamer beacons that light up in the presence of zinc. *Anal. Bioanal. Chem.* **390**, 1067-1075 (2008).
29. Xu, Y. et al. Single-Cell Secretion Analysis via Microfluidic Cell Membrane Immunosorbent Assay for Immune Profiling. *Anal. Chem.* **96**, 49-58 (2023).